Mon. Not. R. Astron. Soc. **283,** 55–65 (1996)

# Ultraviolet spectroscopy of the hotspot in the classical T Tauri star DI Cep: observational indications of magnetically channelled accretion

Ana I. Gómez de Castro[1]★ and Matilde Fernández[2]

[1]*Departamento de Astronomía y Geodesia, Facultad de Ciencias Matemáticas, Universidad Complutense de Madrid, 28040 Madrid, Spain*
[2]*Max-Planck-Institut für Astronomie, Konigstuhl 17, D-69117 Heidelberg, Germany*

Accepted 1996 June 5. Received 1996 May 31; in original form 1995 December 5

**ABSTRACT**

T Tauri stars (TTS) are low-mass pre-main-sequence stars that are accreting mass from the surrounding disc. The hotspots detected in some of them are probably heated by the release of gravitational energy in the accretion of the disc material on to the star. In this work we study the UV spectrum of the hotspot detected in DI Cep to constrain the physical mechanisms heating the spot and to study the possible role of the magnetic field in channelling the accretion flow.

DI Cep is a classical TTS, classified as G8 IV, with a hotspot ($T \sim 8500$ K) covering 1–3 per cent of the visible hemisphere. We have carried out a monitoring campaign with the Short Wavelength spectrograph (1200–2000 Å) and the optical FES Camera of the *International Ultraviolet Explorer* (*IUE*) from 1992 July 12 to 26. The UV spectrum of DI Cep shows excess emission in the continuum from 1700 Å towards longer wavelengths with respect to a G8 IV star. The far-UV spectrum is dominated by strong emission lines of O I, C IV, Si IV, Si II and Si III], with typical surface fluxes of $\sim 10^6$ erg cm$^{-2}$ s$^{-1}$. The UV fluxes (lines and continuum) vary in phase and reach the maximum when the optical flux (FES) does. The light curves are similar in all the lines: the emission from the hotspot is detected above a baseline flux probably produced by the stellar atmosphere. There is a broad range of temperatures in the hotspot (from $10^4$ to $10^5$ K) that is similar to that observed in the plages of magnetically active cool stars (e.g. II Peg). However, in DI Cep the *light curves of the UV lines and continuum are correlated with the optical continuum (V-band) light curve*.

DI Cep as a whole deviates only slightly from active stars in the C IV–Si II and C IV–C II flux–flux relations (there is a factor of 2 excess of Si II with respect to C IV when compared with the regression line fitted to active stars). This suggests that the chromosphere and transition region of DI Cep are heated by a mechanism similar to that of the active main-sequence stars. However, the spot is significantly shifted from these relations in the flux–flux diagrams, displaying an excess of Si II (or a defect of C IV) with respect to the surface fluxes emitted by magnetically active stars. The spot alone radiates as much energy as the rest of the atmosphere, and the spot surface fluxes are $\sim 10^8$ erg cm$^{-2}$ s$^{-1}$ (typically 2 orders of magnitude larger than those corresponding to the atmosphere). Our observations support the theories in which the accreting material is magnetically channelled on to the stellar surface. Variations in the temperature of the spot between observations taken 1 year apart suggest that the infalling material is more likely channelled by a transient loop structure attached to the star than by a strong stellar dipolar field.

The total energy radiated in the far UV lines plus the UV continuum excess is $\geq 0.07\,L_\odot$. This can be accounted for by the accretion of $\geq 6 \times 10^{-9}\,M_\odot$ yr$^{-1}$ from the corotation radius ($8.3\,R_*$).

**Key words:** stars: activity – stars: formation – stars: individual: DI Cep – stars: magnetic field – stars: pre-main-sequence – ultraviolet: stars.

★E-mail: aig@vilspa.esa.es

## 1 INTRODUCTION

T Tauri stars (TTS) are low-mass pre-main-sequence (PMS) stars which are accreting mass from their surrounding discs. The details of this process are not known. The most widely held view proposes that material from a viscous disc accretes steadily on to the star through a boundary layer between the disc and the star (Bertout, Basri & Bouvier 1988, hereafter BBB). This boundary layer is thought to be the source of the UV continuum excess of TTS with respect to main-sequence stars of the same spectral types. Accretion rates of $\sim 3 \times (10^{-6}$–$10^{-8})$ $M_\odot$ yr$^{-1}$ allow us to reproduce reasonably well the spectra of the TTS from the UV to the mid-infrared (BBB; Adams et al. 1987). However, some properties cannot be explained by this simple model.

Some TTS have periodic photometric variability. The periods inferred are 2–10 d, in agreement with those expected for rotational modulation. The periodicity has been explained as being the result of the presence of spots on the stellar surface. The analogy is normally made with the RS CVn systems and, in fact, the properties of many TTS can be explained in a similar way, i.e. by the presence of *dark spots* generated by enhanced solar-like activity. However, there are some objects the properties of which cannot be explained by this mechanism. Some TTS have *much stronger* variations in the *U* than in the *R* or *I* bands, and in these cases the variability is best modelled by hotspots (hot spots) on the stellar surface (Bouvier et al. 1993). A likely source of energy for the hotspots is accretion. In this view, mass infall is channelled by the magnetic field into regions that are heated by the shock of the free-falling material with the stellar surface (Simon, Vrba & Herbst 1990; Königl 1991). Some theoretical models have been developed in recent years, mainly addressing the implications of magnetically channelled accretion in the spin-down of PMS stars and the generation of mass outflows (Tout & Pringle 1992; Cameron & Campbell 1993; Shu et al. 1994; Pearson & King 1995).

Key observational tests, however, have not yet been done. If the material falls on to the stellar surface channelled by the field lines, the UV flux (the accretion flux) variation should be correlated with the optical variability. The correlation between the optical and the UV variability has been studied for two sources so far: BP Tau (Simon et al. 1990) and RU Lup (Giovannelli et al. 1990). A study of the correlation between optical and UV continuum variability has been also carried out for the TTS in Taurus using the *International Ultraviolet Explorer* (*IUE*) archive data (Gómez de Castro et al. 1996). However, these correlations could simply be the result of the well-known flaring activity of the TTS (e.g. Joy 1945; Montmerle et al. 1993), or of accretion instabilities. In general, the rotational period has not been well tracked. For instance, RU Lup was observed just eight times in five years, and BP Tau has a photometric period of around 7 d (Vrba et al. 1986) but only half of this period was well-monitored in the 1200–2000 Å range, where the most prominent resonance lines are observed.

In this work, this problem is addressed by studying the UV flux variations of DI Cep, a classical TTS with a hotspot. The light curves of DI Cep derived from optical photometry, show a smooth variation from the *I* to the *B* band that becomes very steep in *B* and *U*; the observations are reproduced by hotspots with temperatures in the range 7400–8300 K, covering 2.6–1.5 per cent of the visible hemisphere (Fernández & Eiroa 1995). The suggested period is 11 d. We have selected this source because of its UV brightness: $U \simeq 11.6$ mag and $A_V = 0.24$ (Yu et al. 1986) allows us to achieve spectra with signal-to-noise ratios (S/N) $\sim 6$ with the Short Wavelength Prime (SWP) camera (1200–2000 Å) of *IUE* in $\sim 3$ h. The *IUE* data used in this work are presented in Section 2. The UV spectrum of DI Cep is described in Section 3. The main spectral features are identified, and high resolution profiles of the Mg II lines are shown. The overall variability of DI Cep between 1978 and 1992 is studied in Section 4. It is shown that the UV continuum and lines both vary and that the variations are correlated. Then, the results of the *IUE* monitoring of DI Cep from 12 to 26 July 1992 are analysed. It is shown that the light curves are similar for the optical and the UV continuum, and for most of the ultraviolet lines (those originated by ions and neutrals such as C IV, Si II, O I, Si IV, Si III], Si II). It is concluded that there is a broad range of temperatures in the spot ranging from $10^4$ to $10^5$ K: the implications for the accretion mechanism and its possible connection with the stellar activity are discussed in Section 5. A distance to DI Cep of 300 pc (Kholopov 1959) will be assumed throughout this work.

## 2 OBSERVATIONS

Three sets of data are analysed, all of them obtained with *IUE*. A detailed description of the spacecraft configuration at the time when the observations were carried out can be found in Gonzalez-Riestra et al. (1995). In 1992 July we ran a monitoring campaign to observe DI Cep with the SWP camera six times in 15 d (1.25 times the period suggested from optical photometry). In 1992 December, we obtained a high-dispersion spectrum with the Long Wavelength Prime (LWP) camera to study the profile of the Mg II lines. These data sets have been completed with the spectra of DI Cep, available in the *IUE* archive, that were obtained during the first years of *IUE*'s operation (1978–80). Thus, the whole sample consists of 14 spectra: one high-dispersion spectrum obtained with the LWP camera and 13 low-dispersion spectra, two of which obtained with the Long Wavelength Redundant (LWR) camera and 11 with the SWP. The date of observation, camera, image number and exposure time of each spectrum are given in Table 1, as well as the visual magnitude of DI Cep at the beginning of each observation (last column of Table 1). The FES gives estimates of the visual magnitude with rms errors of 0.08 mag and even better rms errors associated with the reproducibility: $\sim 0.04$ mag (Holm & Rice 1981). The FES measurements have been converted into magnitudes using Stickland's (1980) calibration for the 1978–80 data and Pérez's (1991) calibration for the monitoring campaign data. They have been corrected for colour effects, the sensitivity degradation of the cameras (Fireman & Imhoff 1989) and the change of the FES reference point after 1990 July in the European *IUE* Observatory at Villafranca, Spain (VILSPA). The spectra have been processed at VILSPA with the standard software. Each image has been cleaned of bright spots and cosmic-ray hits after visual inspection of the line-by-line spectrum. The data have not been corrected for extinction.

**Table 1.** Log of *IUE* data.

| Date | CIM | $T_{exp}$ (min) | V(FES) (mag) |
|---|---|---|---|
| **Low Dispersion** | | | |
| 19-MAY-78 | LWR01514 | 60 | (1) |
| 26-AUG-78 | LWR02176 | 50 | 11.16 ± 0.04 |
| 23-AUG-78 | SWP02379 | 125 | 11.24 ± 0.04 |
| 25-AUG-78 | SWP02398 | 246 | 11.15 ± 0.04 |
| 28-OCT-80 | SWP10494 | 142 | 11.51 ± 0.04 |
| 08-NOV-80 | SWP10562 | 217 | 11.49 ± 0.04 |
| 09-NOV-80 | SWP10573 | 197 | 11.48 ± 0.04 |
| 12-JUL-92 | SWP45122 | 170 | 11.41 ± 0.02 |
| 16-JUL-92 | SWP45149 | 145 | 11.31 ± 0.02 |
| 18-JUL-92 | SWP45170 | 170 | 11.27 ± 0.02 |
| 22-JUL-92 | SWP45205 | 146 | 11.26 ± 0.02 |
| 24-JUL-92 | SWP45222 | 135 | 11.37 ± 0.02 |
| 26-JUL-92 | SWP45230 | 160 | 11.34 ± 0.02 |
| **High Dispersion** | | | |
| 22-DEC-92 | LWP24555 | 340 | (1) |

(1) No FES counts measured.

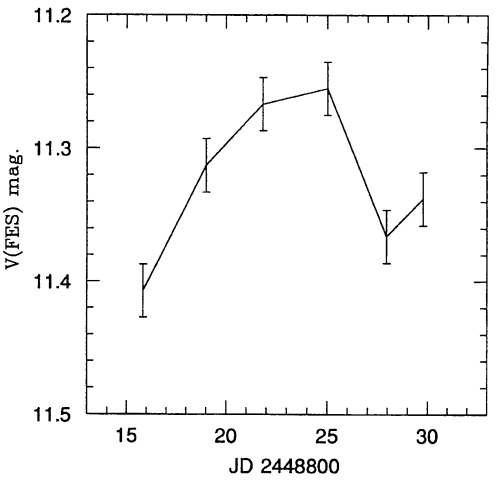


**Figure 1.** FES light curve of DI Cep during the UV monitoring campaign of 1992 July.

We have re-extracted the spectra corresponding to the 1992 monitoring from the line-by-line images provided by the *IUE* Spectral Image Processing System (IUESIPS) to optimize the S/N and get better quality light curves. For this purpose, we have used an extraction slit of only 3 pixel (4.5 arcsec) that contains 99 per cent of the flux, instead of the $9\sqrt{2}$ pixel (19.2 arcsec) slit used in the standard IUESIPS extraction for point sources. In this way the S/N increases by a factor of ~1.5. The spectra have been flux-calibrated using the Bohlin & Holm (1980) calibration.

### 2.1 Optical light curve during the *IUE* monitoring campaign

Optical photometry of DI Cep shows a smooth variability with an amplitude of 0.2 mag in $V$ (Fernández & Eiroa 1995). Measuring accurately such small variations with the FES camera requires differential photometry (Guinan 1990). Therefore, during the 1992 *IUE* monitoring campaign we observed a comparison star of similar spectral type just before observing DI Cep. The improved magnitudes are given in Table 1 for the 1992 SWP observations. The FES light curve during the 1992 monitoring campaign is displayed in Fig. 1. DI Cep was brightening from July 12 until July 24, when the $V$ flux decreased again. The inferred period of ~11 d is consistent with that suggested by ground-based observations. The FES light curve is similar to that obtained by Fernández & Eiroa (1995) and Gahm et al. (1993) between JD 244 5610 and 244 5630.

## 3 THE UV SPECTRUM OF DI CEP

The mean UV spectrum of DI Cep is displayed in Fig. 2. The inset shows in more detail the spectrum between 1200 and 1950 Å. The 1200–1950 Å range is dominated by strong emission lines of O I, Si IV, C IV, He II, Si II, Si III] and C III]. The line identifications are tentative for the weaker features. For instance, high-resolution spectra would be highly desirable around the feature at 1641 Å that we have identified as He II but which could also be O I (UV 146), which shares a common upper level with the strong O I 1304-Å resonance lines. The main spectral feature in the 2000–3200-Å range is the Mg II emission doublet at 2800 Å that is saturated in the two LWR images. The strong Fe II lines at 2507 Å, resulting from the flourescence of Ly$\alpha$, are also clearly seen. Weaker emission features in this range are the C II] and Si II] blend at 2330 Å and the Al II 2670-Å resonance line. The deep absorption at 2580 Å is a reseau mark used for the geometric calibration of the *IUE* images. The main spectral features, their wavelength and mean surface fluxes are given in Table 2. The fluxes have been obtained by Gaussian fitting of the profiles; they have been converted into fluxes at the stellar surface, adopting a radius of 2.5 $R_\odot$ (Hamman & Persson 1992).

The overall spectrum is fairly similar to those found in magnetically active stars such as some cool dwarfs, dMe or RS CVn stars. DI Cep has been classified as a G8 IV star (Gahm & Petrov 1983). G8 stars have a cut-off in the energy distribution at ~2900 Å, the stellar flux decreasing sharply from this point towards shorter wavelengths. The brighter LWR spectrum of DI Cep is compared in Fig. 3 with the spectrum of three G8 standards of luminosity classes V, IV and III from the *IUE* Low Dispersion Catalogue. These are HD 10700 (G8 V), HD 188512 (G8 IV) and HD 43039 (G8 III). The standard spectra have been normalized to the DI Cep (LWR 1514) flux in the range 3000–3200 Å for this plot. DI Cep clearly shows an excess of emission at wavelengths shorter than 2900 Å with respect to these stars. The UV spectra of G8 stars vary with the luminosity class. The UV continuum at $\lambda \leq 2850$ is fainter, with respect to the continuum at $\lambda \geq 2850$, in the class III than in the class V sources. It is clear from the spectra that the extended atmosphere of the cool giants does not simulate well, in the UV, the rarified and warm environment around DI Cep. In fact, the spectrum of HD 10700 is the most similar to that of DI Cep. However, the DI Cep spectrum is less steep in the 2900–3200 Å range and the relative strength of Si III is greater, indicating a lower electron-density regime in DI Cep than in main-sequence stars. The large relative strength

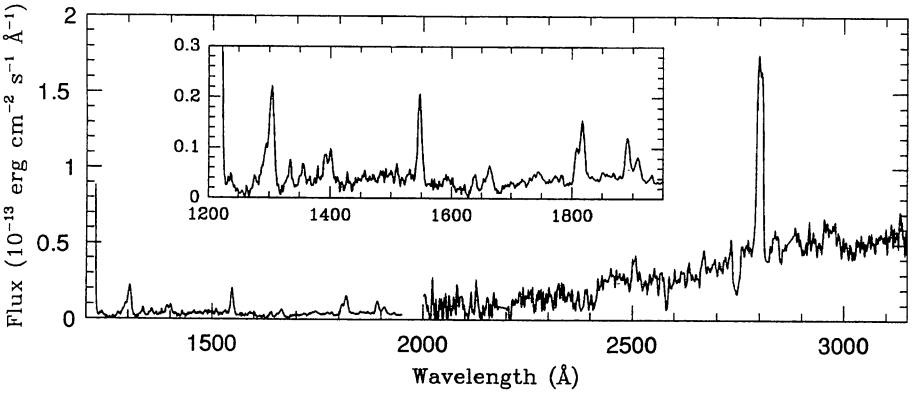


**Figure 2.** Mean UV spectrum of DI Cep.

**Table 2.** Main spectral lines in the SWP spectrum.

| λ (Å ) | Specie | Flux($10^6$ erg cm$^{-2}$ s$^{-1}$) |
|---|---|---|
| 1238,1242 | N V (UV1) | 0.90 |
| 1303 | O I, Si III (UV4) | 6.24 * |
| 1335 | C II (UV1) | 0.84 |
| 1355 | O I | 1.06 |
| 1393,1402 | Si IV (UV1) | 2.60 |
| 1548,1551 | C IV (UV1) | 4.35 |
| 1591.1 | Fe II | 0.71 |
| 1640 | He II | 0.85 |
| 1665 | CI (UV3), Al II(UV2) | 2.02 * |
| 1808,1817 | Si II(UV3) | 4.18 |
| 1892 | Si III ] | 2.17 |
| 1909 | C III ] | 1.30 |

*Uncertain fluxes because of blending.

of the O I resonance lines with respect to the rest of the spectral features also suggests a lower gravity in DI Cep. The O I emission is enhanced by the greater opacity to Ly$\beta$ photons in lower gravity stars.

The comparison between DI Cep and HD 10700 makes more conspicuous some emission bumps at 2200–2400, 2400–2600 and 2700–2900 Å. They are produced in part by the Fe II emission lines corresponding to the multiplets: UV 2, 3, 35, 36 (2330–2410 Å); UV 32, 62, 63 (2700–2750 Å); UV 60, 78 (2900–3000 Å). Note that, although the Fe II lines are individually weaker than the Mg II, C II or Si II lines, they are so numerous that, combined, they become a significant coolant of the chromospheres of the PMS stars (see e.g. Jordan 1988). In addition to the lines, there seems to be an underlying continuum that represents the high-energy tail of the optical veiling continuum. The far UV (FUV) (1200–2000 Å) spectrum of DI Cep also shows a weak continuum composed of two bumps centred at 1500 and 1850 Å. From 1750 Å towards longer wavelengths we observe the high-energy tail of the LWR continuum excess. The continuum between 1400 and 1600 Å could be due to the blending of many weak emission lines from metals. The 1500-Å bump is strongly reminiscent of that observed in the high-excitation Herbig–Haro (hereafter HH) objects like HH 2; the SWP spectrum of HH 2H is displayed in Fig. 4 for comparison. This suggests that the same physical processes which excite the HH nebulosities may be occurring in the circumstellar medium around DI

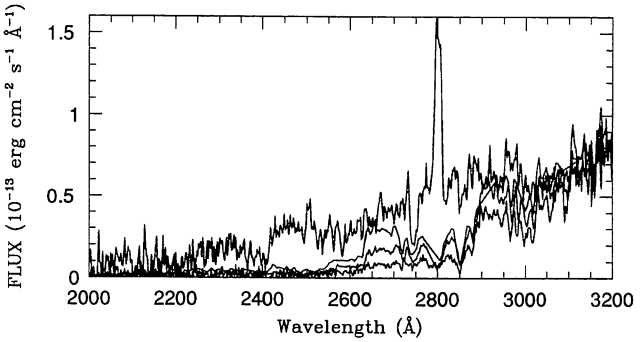


**Figure 3.** LWR 1514 spectrum plotted against the 2000–3200 Å spectrum of standard G8 stars of luminosity classes V, IV and III. The UV continuum below 2900 Å decreases as the luminosity increases. All the spectra are normalized to DI Cep flux in the range 3000–3200 Å.

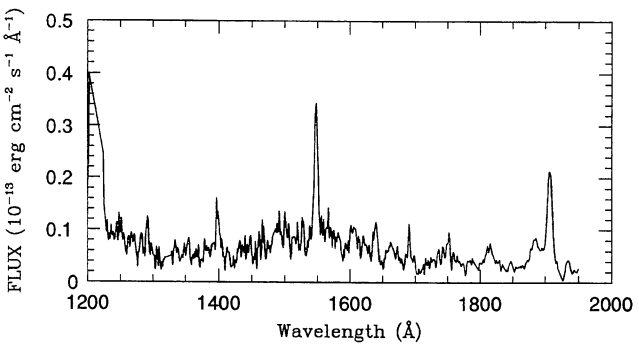


**Figure 4.** SWP spectrum of HH 2 H (SWP 40663).

Cep. The unexpected strong far-UV continuum of HH objects was usually interpreted as the collisionally enhanced two-photon emission of hydrogen (Dopita & Schwartz 1981), although the true nature of the emission mechanism remains somewhat uncertain (Imhoff & Appenzeller 1987).

### 3.1 The Mg II lines profiles

The Mg II lines only have S/N$\simeq$10 in the high-resolution spectrum; they are observed over a weak continuum that extends from 2700 Å towards longer wavelengths. The lines

have a P Cygni profile with a broad blueshifted absorption component and a redshifted asymmetric emission component (see Fig. 5) that is characteristic of line formation in an expanding envelope. An upper limit to the terminal velocity of the wind of $\sim -410$ km s$^{-1}$ is derived from the Mg II line at 2795 Å. Note that the low-level continuum and the presence of some metallic lines makes it very difficult to determine the precise point at which the blue wing merges into the continuum (see e.g. Talavera & Gómez de Castro 1987). The ratio between the emission components of the *h* and *k* lines indicates that they are formed in optically thick plasma. There is a saturated narrow absorption feature superimposed on the emission component, probably as a result of warm circumstellar gas. Finally, note that the emission component has a broad wing to the red extending up to 2.8 Å (300 km s$^{-1}$).

The Mg II lines of the TTS usually show P Cygni profiles [see Imhoff & Appenzeller (1987) for a review]. In this context, DI Cep represents an intermediate type between GW Ori (a moderate-emission TTS) and RW Aur (a strong-emission TTS). The Mg II lines of GW Ori are optically thin, and the narrow circumstellar-absorption component is not saturated as in DI Cep. However, in DI Cep the blueshifted component of the P Cygni profile is not filled in with emission as it is in RW Aur.

## 4. UV VARIABILITY

The UV spectra of DI Cep are displayed in Fig. 6(a) and (b) for the LWR and SWP cameras, respectively. The integrated flux in the spectral range 2200–3100 Å (excluding the Mg II line) is 32 per cent higher in the LWR 1514 image than in the LWR 2176. The UV excess of DI Cep in the LWR 1514 image with respect to the LWR 2176 is $> 0.064$ $L_\odot$ (no extinction correction has been applied). The ratio and the difference between the two images are plotted in Fig. 7. The ratio declines towards shorter wavelengths and peaks between 2800 and 3000 Å. It is not flat, indicating that the energy distribution changes: the variability is not just produced by an increment of the stellar luminosity as a whole. Provided that the variations between the two LWR images (taken few months apart) are the result of the visibility of the spot, the difference between the LWR 1514 and 2176 images shows up the spectral distribution of the energy radiated by the spot. The emission bumps at 2200–2400, 2400–2600 and 2700–2900 Å are clearly identified (see Section 3). Therefore the excess emission with respect to main-sequence stars at wavelengths shorter than 2900 Å is the result, at least in part, of the contribution of the hotspot. There is no optical photometry simultaneous with the LWR *IUE* observations, hence we cannot determine from these data alone whether, in the minimum of the photometric cycle, DI Cep has an excess in the UV-continuum emission with respect to main-sequence stars of similar spectral types.

The SWP continuum and line emission are also variable. The only lines that are strong enough to be clearly measured

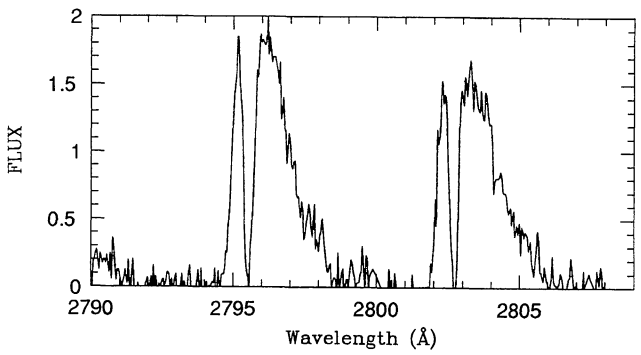


**Figure 5.** Mg II line profiles. The flux is given in arbitrary units.

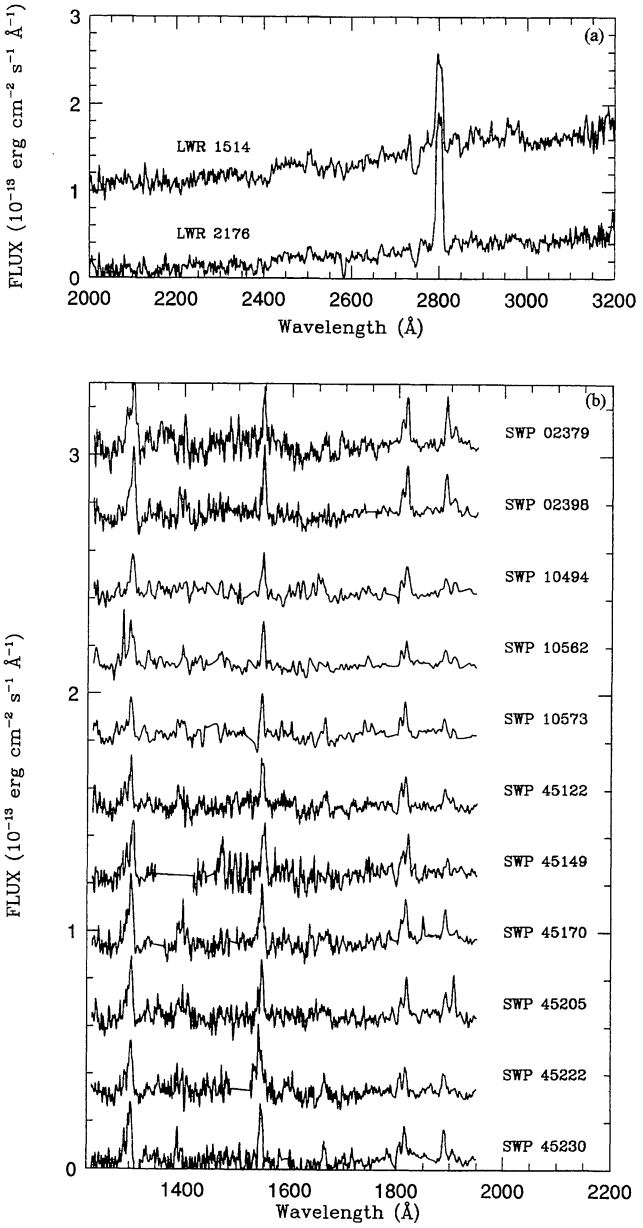


**Figure 6.** (a) LWR and (b) SWP spectra of DI Cep. The flux scale in panels (a) and (b) applies to the spectra of LWR 2176 and SWP 45230 respectively. The following offsets have been applied to the rest of the spectra: $1 \times 10^{-13}$ erg cm$^{-2}$ s$^{-1}$ Å$^{-1}$ to the LWR 1514 spectrum in panel (a) and 0.3, 0.6, 0.9, 1.2, 1.5, 1.8, 2.1, 2.4, 2.7 and $3.0 \times 10^{-13}$ erg cm$^{-2}$ s$^{-1}$ Å$^{-1}$ to the spectra in panel (b), in increasing order from the SWP 45222 to the SWP 02379 spectra.

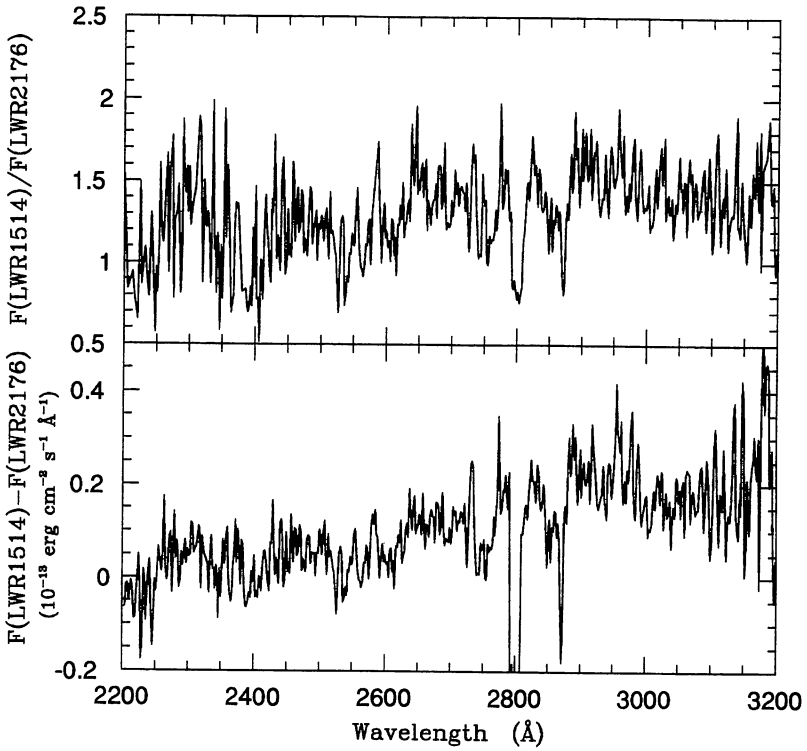


**Figure 7.** Top: rate between the LWR 1514 and 2176 spectra. Bottom: difference between the LWR 1514 and 2176 spectra.

**Table 3.** Spectral windows defined on the DI Cep spectrum.

| No. | Wavelength Range $\lambda_i, \lambda_e$ (Å ) | Ident. |
|---|---|---|
| 1 | 1294,1312 | O I |
| 2 | 1382,1416 | Si IV |
| 3 | 1440,1520 | Continuum |
| 4 | 1537,1555 | C IV |
| 5 | 1720,1785 | Continuum |
| 6 | 1802,1825 | Si II |
| 7 | 1830,1880 | Continuum |
| 8 | 1880,1900 | Si III ] |
| 9 | 1900,1915 | C III ] |

in all the spectra are those from O I, C IV, Si II and Si III]; also Si IV and C III] lines are seen in many individual spectra. To measure their variations, we have defined nine windows whose characteristics are summarized in Table 3. Some of them are dominated by strong emission lines, while others are centred in the continuum bumps. We have computed the total fluxes per window for each spectrum. The S/N in the 1400–1600 Å continuum band is very poor in the individual spectra and cannot be used for variability studies; only the continuum window at 1830–1880 Å is suitable for this purpose. The results are given in Table 4. The image number is given in the first column, the second column gives the mean flux per angstrom in the 1830-Å continuum window, and the rest of the table gives the total fluxes in the O I, Si IV, C IV, Si II, Si III] and C III] windows. The flux values affected by cosmic ray hits that could not be properly cleaned are indicated. An estimate of the error in the line fluxes has been derived from the standard deviation from the mean in the continuum window, 1830–1880 Å. The continuum contribution to the total flux in the Si II, Si III] and C III] windows has been subtracted out by linear interpolation from the nearby continuum windows. The fluxes in Table 4 are corrected for the sensitivity degradation of the SWP camera (Garhart 1992).

As shown in Fig. 8, the UV- and V-continuum flux variations are correlated. The correlation coefficient is 0.72. The variations are more dramatic in the UV, where the contribution of the stellar atmosphere to the total flux is very small. This confirms the trend found from optical photometry, in which the contribution of the emission region in *U* is found to be variable while in *V* is negligible (e.g. Gahm & Petrov 1983). The O I, Si IV, C IV and Si II line flux variations are also correlated with the UV and optical continua. A similar behaviour has been reported for BP Tau (Simon et al. 1990) and RU Lup (Giovanelli et al. 1990) and seems to be a general trend in the TTS (Gómez de Castro et al. 1996). These long term variations could be the result either of rotational modulation or of the flaring activity of DI Cep. DI Cep is a well-known variable in time-scales as short as a few hours, with a high flaring activity that could be causing these variations (Kholopov 1952; Cohen & Schwartz 1976; Bastian & Mundt 1979; Gahm & Petrov 1983; Kelemen 1985). The largest flares are characterized by rise times of minutes to hours and fall times of several hours.

### 4.1 The UV monitoring campaign

As displayed in Fig. 9, all the lines and the continuum vary approximately in phase during the 15 days that the UV monitoring lasted. The *V*-flux light curve has two minima, on July 12 and 24 (see Fig. 1). In between, the flux is high

**Table 4.** UV lines and continuum fluxes for the individual spectra.

| CIM | $F_{1830-1880}$ $10^{-13}$ erg cm$^{-2}$ s$^{-1}$ Å$^{-1}$ | UV lines fluxes ($10^{-13}$ erg cm$^{-2}$ s$^{-1}$) | | | | | |
|---|---|---|---|---|---|---|---|
| | | O I | Si IV | C IV | Si II | Si III ] | C III ] |
| SWP2379 | 0.047±0.015 | 4.83±0.48 | | 2.44±0.27 | 2.09±0.35 | 1.50±0.30 | 0.70±0.23 |
| SWP2398 | 0.072±0.011 | 4.07±0.37 | 2.30±0.32 | 2.76±0.21 | 1.80±0.26 | 1.28±0.23 | 0.47[1]±0.17 |
| SWP10494 | 0.025±0.009 | 2.25±0.30 | | 1.54±0.17 | 1.39± 0.22 | 0.71±0.19 | 0.50[1]±0.14 |
| SWP10562 | 0.033±0.008 | 3.33[2]±0.27 | 0.93[1]±0.24 | 1.58±0.15 | 1.01± 0.19 | 0.49±0.17 | 0.22[1]±0.13 |
| SWP10573 | 0.047±0.011 | 2.45±0.36 | 1.55[1]±0.31 | 1.52± 0.20 | 1.08± 0.26 | 0.24±0.22 | |
| SWP45122 | 0.033±0.008 | 2.74± 0.27 | 1.24[1]±0.23 | 1.51± 0.15 | 1.17± 0.19 | 0.58± 0.17 | 0.22[1]± 0.13 |
| SWP45149 | 0.047±0.015 | 3.62[2]±0.47 | 2.32± 0.41 | 2.08± 0.27 | 1.67± 0.34 | 0.42[1]± 0.30 | |
| SWP45170 | 0.078±0.011 | 4.37± 0.34 | 2.51± 0.30 | 2.45± 0.19 | 1.67± 0.25 | 0.72± 0.22 | 0.26[1]± 0.16 |
| SWP45205 | 0.054±0.011 | 3.51± 0.36 | 1.93± 0.32 | 2.12± 0.20 | 1.57± 0.26 | 0.53± 0.23 | 1.01± 0.17 |
| SWP45222 | 0.032±0.008 | 3.00± 0.25 | 1.63± 0.21 | 1.73± 0.14 | 1.05± 0.18 | 0.43± 0.15 | |
| SWP45230 | 0.054±0.011 | 3.81± 0.36 | 1.70± 0.32 | 2.07± 0.20 | 1.51± 0.26 | 0.66± 0.23 | 0.27[1]± 0.17 |

(1) Very weak feature.
(2) Dubious: bright nearby feature on the spectrum, likely a cosmic ray.

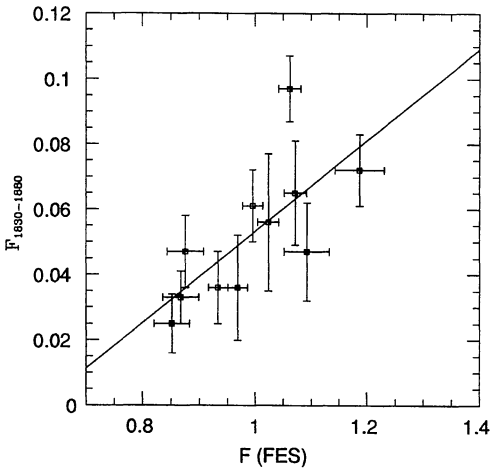


**Figure 8.** Correlation between UV and V continuum variations.

and remains quite constant. The UV-continuum flux peaks between July 16 and 22 as the O I, Si IV, C IV and Si II lines do. The singly ionized species and the continuum excess are characteristics of plasma at $\sim 10^4$ K, while C IV, Si IV, N V and He II are formed in gas at $\sim 10^5$ K. There seem to be slight variations in the shape of the light curves for the different species but it will be necessary to obtain spectra with better S/N to confirm them. The only clearly significant difference is between the C III] line and the rest of the lines and continua. Note that C III] is very weak during the entire period except for July 22, when it becomes one of the most prominent features, reaching S/N = 6. The differences between the light curves suggest that the detailed thermal structure of the hotspot could be resolved with a better S/N and time resolution of the rotation period. The similarity between the light curves of the UV continuum and of the UV lines points out that there is significant line emission from the hotspot. In the star–spot model, the hotspot is assumed to be on the stellar surface and to radiate as a blackbody. In this context, our observations indicate that there is a column of highly excited gas over the hotspot,

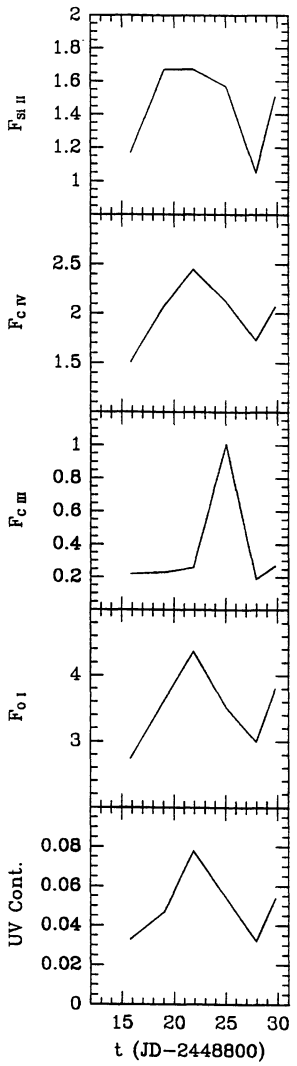


**Figure 9.** Light curves of the UV continuum (1830–1880 Å) and the more significant spectral features obtained during the *IUE* monitoring campaign.

heated by other mechanisms in addition to the spot thermal radiation.

In general, active stars show variations of their UV-line fluxes as a result of the presence either of plages or of flares (see review by Linsky 1991 and references therein). Well-studied systems of this type are V711 Tau, AR Lac and II Peg. During the flares, the line fluxes increase dramatically in a few hours [for instance, in the 1981 October flare of V711 Tau, the C IV flux rose by a factor of 340 with respect to the pre-flare value (Rodonó et al. 1987)]. The plages, however, last for more than a rotational period and are responsible for a much milder and rotationally modulated variability. A well-studied source of this kind is the RS CVn system II Peg (Rodonó et al. 1987), in which the C IV flux varies by a factor of 1.5 between the maximum and the minimum, while the fluxes of singly ionized species (Si II, Mg II) vary by only 20 per cent (or even less). However, the main difference between DI Cep and active cool stars is that the optical light curves, and those corresponding to the spectral tracers of chromospheres and transition regions, are correlated in DI Cep, while in active stars the Mg II and Ca II line fluxes peak when the visual flux is at minimum, indicating that hot regions in the chromosphere and cool photospheric spots are spatially correlated (as would be expected if they are both magnetic structures).

Finally, note that there is a background level different from 0 in all the light curves. This background emission could be the result either of emission from the stellar atmosphere (chromosphere or transition region) or of the visibility of the hotspots, which in turn depends on their latitude and on the star inclination. Unfortunately, the data available in the literature are not sufficiently coherent to allow us to derive from them the DI Cep inclination. The projected rotational velocity measured by Gameiro & Lago (1993), $V\sin(i)=23.0\pm4.3$ km s$^{-1}$, is too large when compared to that derived from the uncertain rotational period of 11 d and the stellar radius of 2.5 $R_\odot$, which yields to $V=4.6\times R_*(R_\odot)$ km s$^{-1}$. Note, however, that the only line that does show a 0 background level in the light curve is the semiforbidden C III] line, which is not usually observed in the magnetic structures of main-sequence stars because of their density regime ($N_e\geq10^{10}$ cm$^{-3}$ and $T_e\simeq50\,000$ K). This suggests that the background levels in the light curves of the other species are due to atmospheric emission and that the hotspot is totally occulted during part of the rotational period. This also agrees with the results of the optical study by Gahm & Petrov (1983), who showed that there is no or very little optical veiling in the most quiescent phase of DI Cep; this optical veiling represents the low-energy tail of the UV excess.

## 5 DISCUSSION

### 5.1 Thermal structure of the hotspot

The broad range of temperatures observed in the hotspot of DI Cep is much like that observed in the plages associated with the *dark spots* in the atmospheres of magnetically active stars, such as II Peg. This is intriguing, and makes us wonder whether there is any connection between the mechanisms that heat the hotspot and the magnetic activity of the TTS in general, and DI Cep in particular. Unfortunately, the signatures of each possible heating mechanism, that is the thermal response of the gas to heating, are not easy to find. The observational tool most often used to gain insight into this problem is the study of the correlations between the fluxes of lines formed in the chromosphere, transition region and corona (henceforth flux–flux correlations) and between these fluxes and the stellar rotation period (flux–period correlations). In particular, if the heating rate for a class of stars correlates with the rotation period or the Rosby number, the heating mechanism is probably magnetic in character. The details of the physical mechanism by which the stellar rotation energy is transferred to the magnetic field enhancement, and from there dissipated into the heating of low-density media, are still under debate (see e.g. Jordan 1991). The clue seems to be in the relationship between the observed activity and the dynamo action in the subphotospheric convection zone which is thought to be the underlying cause of activity.

The TTSs extend the flux–flux and flux–period correlations, as defined by other cool stars, towards larger flux densities, typically by a factor $\sim$40. The TTS also show a relatively low strength of the high-ionization lines with respect to the low-ionization ones when compared with main-sequence stars (Imhoff & Appenzeller 1987). The extrapolation of the flux–flux relationships towards the TTS region has led Lemmens, Rutten & Zwaan (1992) to claim that classical TTS do not follow the same flux–flux relations as do the rest of the active stars: F, G, K dwarfs, dMe stars, RS CVn and even the weak lines TTS. The position of DI Cep in the Si II–C IV and the C II–C IV flux–flux diagrams is plotted in Fig. 10. All values corresponding to the *IUE* monitoring campaign are plotted in the Si II–C IV plot, and only a mean value is used in the C II–C IV plot since the S/N of C II is low in the individual spectra. The two concentrations of data points correspond to Si II and C IV values at minimum (lower fluxes) and at maximum (higher fluxes). The data for late-type stars have been extracted from Rutten (1987) and Rutten et al. (1991), and only sources with accurate C IV flux have been included. The nearest source to DI Cep is HD 117555, a G2 III star with a rotation period of 2.41 d. Note that DI Cep does not deviate significantly from the flux–flux relations of the active stars, and that it is only slightly shifted from the active star-correlation line in the Si II–C IV diagram: there seems to be an excess of Si II emission with respect to C IV, but given the large dispersion of the active stars around the least-squares-fit line (see Fig. 10) the excess may not be significant. Therefore, the chromosphere and transition region of DI Cep could be heated by enhanced magnetic activity. Note that DI Cep lies above the saturation limit; a saturated atmosphere is characterized by the maximum observed emission in chromosphere, transition region and corona spectral indicators. The presumption is that saturated stars have magnetic filling factors close to unity and, in this case, magnetic heating determines the saturated heating rates (see e.g. review by Linsky 1991).

The Si II and C IV fluxes radiated by the hotspot alone can be calculated making use of the size of the hotspot determined from optical photometry. *UBVRI* photometry carried out just 10 d after the *IUE* campaign shows that the hotspot has an area of between 0.026 and 0.015 of the visible hemisphere (Fernández & Eiroa 1995). The derived fluxes are

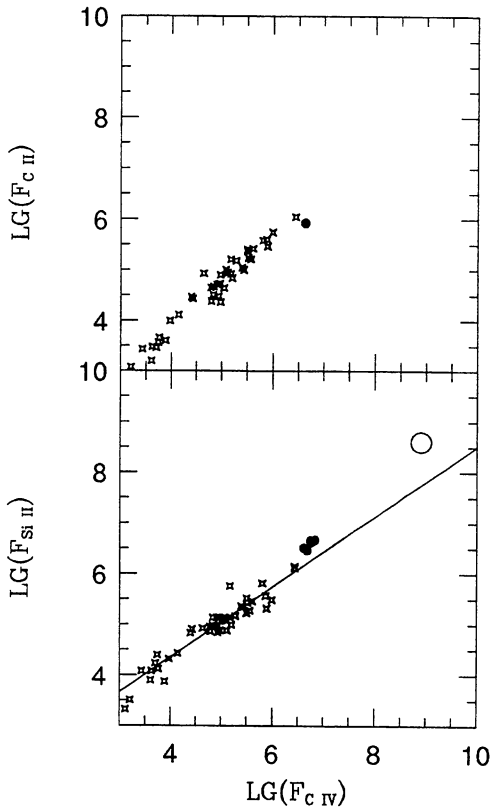


**Figure 10.** C II–C IV (top) and Si II–C IV (bottom) flux–flux relations for magnetically active stars. The mean location of DI Cep in the C II–C IV diagram is indicated by a filled circle (top). All values corresponding to the *IUE* monitoring campaign are plotted in the Si II–C IV plot, also with filled circles. The location of the hot spot is indicated by a big open circle.

$F(\mathrm{C\,IV}) = (8.0\text{–}8.3) \times 10^8$ erg cm$^{-2}$ s$^{-1}$ and $F(\mathrm{Si\,II}) = (4.0\text{–}4.2) \times 10^8$ erg cm$^{-2}$ s$^{-1}$, that is, around 2 orders of magnitude larger than those radiated by the atmosphere as a whole, pointing out that there are extended magnetic structures associated with the hotspot. It is unfortunate that the light curves in Fig. 9 are not good enough to use to look for differences in the visibilities of the regions where high ionization and singly ionized species are formed. The location of the hotspot in the flux–flux diagram is marked with a big circle in Fig. 10. Note that the hotspot deviates more from the flux–flux relation of the active stars than does the atmosphere, suggesting that the excitation mechanisms are different. Yet the hotspot is fairly close to the correlation line, which is intriguing since the physical mechanisms involved in the heating of the gas seem to be very different from *magnetic activity*: the hotspot is heated by the release of gravitational energy by the infalling material.

### 5.2 Magnetically channelled accretion?

A hot boundary layer between the star and the accretion disc cannot account for the presence of hotspots associated with regions at $T \sim 10^5$ K. Current accretion disc models cannot account for regions as hot as $10^5$ K, since the hottest regions are the boundary layers, with temperatures between 7000–11 000 K (Basri & Bertout 1993), and have typical time-scales for the development of instabilities of ~12 h.

The presence of a hotspot can be naturally explained if the star has a strong enough magnetic field to channel the accreting gas. Two basic models have been proposed, depending on the field geometry and strength. The protostar may have a strong dipolar magnetic field that channels the disc material towards the magnetic poles (Königl 1991; Cameron & Campbell 1993). Another possibility is the presence of a transient magnetic loop structure attached to the star that drives the inflow towards the loop footpoints by the drag force of the field on the infalling, presumably diamagnetic, material (Pearson & King 1995).

In the first approach, material from the accretion disc shocks with the stellar photosphere heating the gas to temperatures of up to $\sim 10^6$ K in the impact regions (Königl 1991) where the gravitational energy is finally released into heating. The field required at a distance $r$ from the star to stop the free-fall perpendicular to the field and to channel the gas to the magnetic pole is:

$$B(G) = 1.39 \times 10^2 \left(\frac{M_*}{\mathrm{M}_\odot}\right)^{1/2} \left(\frac{r}{R_*}\right)^{-1/2},$$

where $R_* = 2.5\,\mathrm{R}_\odot$. Königl (1991) estimated that the *photospheric field* necessary to drive the accretion flow is $10^3$ $G$; this calculation is based on the scaling of the Ghosh & Lamb (1979) model for TTS. These fields are well within the observational limits (Phillips et al. 1991). Grinin et al. (1980) found strong variations of the polarization spectrum of DI Cep occurring during small ($\Delta V \leq 0.2$ mag) brightness variations that were connected with the shape of the emission spectrum. This suggests that a significant fraction of the DI Cep polarization could be produced in an electron envelope attached to the magnetic field as a result of the effect of Faraday rotation of the plane of polarization. The observed variations could be explained by the influence of variable magnetic fields (either intrinsically variable or with a variable projection in the line of sight as a result of the stellar rotation). The derived field for DI Cep, assuming a bipolar stellar field, is 200–600 G (Gnedin et al. 1988), which is well within the limits required to channel the inflow. In this strong field approach, all the material within the magnetosphere rotates like a rigid body and falls towards the stellar surface from the inner border of the disc at free-fall speed. The disc does not reach the stellar surface because it is disrupted by the magnetosphere. The corotation radius between the star and the disc material, $r$, sets the inner border of the disc. If the disc is Keplerian then

$$r = 8.32\,R_* \left(\frac{M}{\mathrm{M}_\odot}\right)^{1/3} \left(\frac{P}{11\,\mathrm{d}}\right)^{2/3},$$

where $P$ is the rotational period of the material at the inner disc radius. Therefore,

$$V_{\mathrm{ff}} = 140\ \mathrm{km\ s^{-1}} \left(\phi \frac{8.32\,R_*}{r}\right)^{1/2},$$

where $\phi = (M/\mathrm{M}_\odot)(R_*/2.5\,\mathrm{R}_\odot)^{-1}$. If all the kinetic energy were dumped into heating at the shock front, the temperature would be $\sim 1.1 \times 10^6$ K. The total UV luminosity excess

of DI Cep (including line emission) is $\geq 0.07\,L_\odot$ and rises up to $0.1\,L_\odot$ if the fluxes are extinction corrected using the ISM extinction. This energy is equivalent to that released by the accretion of $\geq 6 \times 10^{-9}\,M_\odot\ yr^{-1}$ from the corotation radius. Our observations indicate that there should be a wide range of temperatures in the hotspot generated by the shock; from the 7400–8300 K inferred from the optical photometry to $10^4$ and $10^5$ K of the UV emission-line regions. Yet current models do not explain how such a broad range of temperatures as that observed in DI Cep can be produced.

Large transient radio-loop structures have been resolved in weak-line TTS (WTTS) reaching up to $12\,R_\odot$ (Phillips et al. 1991). However, the precise manner in which the drag force exerted by the loops affects the temperature of the infalling gas is not known. Neither is it clear why such a broad range of temperatures should be observed associated with the loop. Note, however, that loops are expected to be transient structures. The *UBVRI* photometry of DI Cep shows significant variations between 1991 August and 1992 August (Fernández & Eiroa 1995). In 1991 there was a very prominent excess in the *U* band that was not accompanied by a similar excess in the other bands, while in 1992 the excess was more uniformly distributed over all the spectrum. In fact, the energy distribution of the 1992 data can be nicely fitted by a model of a hotspot emitting like a blackbody with temperatures between 7400 and 8300 K, while it is impossible to fit the 1991 data with only this hotspot. The presence of very hot plasma at temperatures that may reach $10^5$ K is required. Moreover, there are significant variations in the optical light curves obtained in 1982, 1983 (Gahm et al. 1993), 1991 (Fernández & Eiroa 1995) and 1992 (Fernández & Eiroa 1995; Gullbring & Gahm 1996; the present work), although sporadically (three times) a light curve is observed similar to the one we monitored with the FES camera. This suggests that there may be transient loop structures in DI Cep, although continuous monitoring for several months is required to confirm the duration of the hotspot.

Given the role that magnetic fields may play in channelling the inflow, distinguishing between dissipative effects associated with magnetic activity or accretion may be extremely difficult in low-mass PMS stars. This, in turn, complicates the interpretation of the standard spectral indicators of magnetic activity. Note that viscous magnetic stresses and gas infall may stir the magnetopause field, producing waves of a nature similar to that responsible for the chromospheric heating in the active stars.

## 6 CONCLUSIONS

The UV spectrum of DI Cep is different from that expected for a G8 IV star. There is an excess emission in the continuum from 1700 Å towards longer wavelengths whose integrated luminosity is $\sim 0.07\,L_\odot$. Also, a broad emission bump has been detected at 1500 Å that is strongly reminiscent of the one observed in high-excitation HH objects. The far-UV spectrum is dominated by strong emission lines of O I, C IV, Si IV, Si II and Si III] with typical surface fluxes of $\sim 10^6$ erg cm$^{-2}$ s$^{-1}$. The Mg II lines have P Cygni profiles pointing out the presence of a wind at the base of the chromosphere with a terminal velocity of the order of $\sim 400$ km s$^{-1}$. The UV continuum and line fluxes are variable, and their variations are correlated with those in the *V* band (derived from FES measurements).

The UV flux (lines and continuum) vary in phase. The light curves are similar in all the species: the emission from the hotspot is detected over a baseline flux produced by the stellar atmosphere. There is a broad range of temperatures in the hotspot (from $10^4$ to $10^5$ K) which is similar to that observed in the stellar atmosphere.

DI Cep deviates slightly from active stars in the C IV–Si II and C IV–C II flux–flux relations (there is a factor of 2 excess of Si II with respect to C IV when compared with the regression line fitted to active stars). However, the hotspot is significantly shifted from these relations in the flux–flux diagrams, displaying an excess of Si II (or a deficit of C IV) with respect to the surface fluxes emitted by magnetically active stars. The hotspot alone, with a size of 1–3 per cent of the visible stellar hemisphere, radiates as much energy as the rest of the atmosphere, suggesting that it is associated with large magnetic structures.

In the current scenario proposed for classical TTS, one should look for these regions in the hottest component of the accretion disc but both time-scales and temperatures are different from those predicted by the generally adopted models. Our observations suggest that both the hotspot and the high-temperature regions result from accretion shocks as a result of a magnetically channelled accretion. Our data alone cannot distinguish between mass infall channelled by a strong dipolar field (e.g. Cameron & Campbell 1993) or by magnetic drag force due to transient magnetic loops (e.g. Pearson & King 1995). Higher resolution observations during a longer time-span are required to confirm that the loop structure is transient. Also, theoretical models of the expected temperature structure of the infalling gas are needed.

## ACKNOWLEDGMENTS

We thank Ed Guinan for suggesting the use of differential photometry, Charo González-Riestra for helping us in the optimal extraction of the *IUE* data, and Domitilla De Martino and John Fernley for their assistance during the observations. AIG also wants to thank Benjamín Montesinos, Brendan Byrne, Richard Henriksen, Michel Tagger and Thierry Foglizzo for many interesting conversations on stellar activity and the role that magnetic fields may play in channelling the inflow from accretion discs. This research was partially supported by the Ministerio de Educación y Ciencia of Spain through a re-entry fellowship to AIG, a pre-doctoral fellowship to MF and research grant PB 93-0491. Most of this work was carried out while AIG was a postdoctoral re-entry fellow in the *IUE* Observatory at VILSPA.

This work is based on observations carried out with the *International Ultraviolet Explorer* (*IUE*) satellite.

## REFERENCES

Adams F. C., Lada C. J., Shu F. H., 1987, ApJ, 312, 788

Basri G., Bertout C., 1993, in Levy E. H., Lunine J. L., eds, Protostars & Planets III. The University of Arizona Press, Tucson, p. 543

Bastian U., Mundt R., 1979, A&A, 78, 181
Bertout C., Basri C., Bouvier J., 1988, ApJ, 330, 350 (BBB)
Bohlin R. C., Holm A., 1980, NASA IUE Newsl., 10, 37
Bouvier J., Cabrit S., Fernández M., Martín E. L., Matthews J. M., 1993, A&A, 272, 176
Cameron A. C., Campbell C. G., 1993, A&A, 274, 309
Cohen M., Schwartz R. D., 1976, MNRAS, 174, 137
Dopita M. A., Schwartz R. D., 1981, PASP, 93, 546
Fernández M., Eiroa C., 1995, A&A, 310, 143
Fireman G. F., Imhoff C. L., 1989, NASA IUE Newsl., 40, 10
Gahm G. F., Petrov P. P., 1983, in Byrne P. B., Rodonó M., eds, Activity in Red-Dwarf Stars. Reidel, Dordrecht, p. 497
Gahm G. F., Gullbring E., Fischerström C., Lindroos K. P., Loden K., 1993, A&AS, 100, 371
Gameiro J. F., Lago M. T. V. T., 1993, MNRAS, 265, 359
Garhart M. P., 1992, 3 Agency Meeting Report, VILSPA, 12 Jun 1992
Ghosh P., Lamb F. K., 1979, ApJ, 234, 296
Giovannelli F., Rossi C., Errico L., Vittone A. A., Bisnovatyi-Kogan G. S., Kurt V. G., Sheffer E. K., Lamzin S. A., 1990, in Rolfe E. J., ed., ESA SP-310, Evolution in Astrophysics. ESA Publications, ESTEC, Noordwijk, p. 231
Gómez de Castro A. I., Monier R., Franqueira M., 1996, in preparation
Gnedin, Yu N., Red'kina N. P., Tarasov K. V., 1988, SvA, 32, 186
Gonzalez-Riestra R., de Martino D., Hermoso D., Barylak M., Rodriguez P., Wamsteker W., 1995, ESA IUE Newsl., 45, 7
Grinin V. P. et al., 1980, Perem. Zvezdy, 21, 247
Guinan E., 1990, in Rolfe E. J., ed., ESA-SP 310, Evolution in Astrophysics. ESA Publications, ESTEC, Noordwijk, p. 73
Gullbring E., Gahm G. F., 1996, A&A, 308, 821
Hamann F., Persson S. E., 1992, ApJS, 82, 247
Holm A., Rice G., 1981, NASA IUE Newsl., 15, 74
Imhoff C. L., Appenzeller I., 1987, in Kondo Y., ed., Exploring the universe with the IUE satellite. Reidel, Dordrecht, p. 295
Joy A. H., 1945, ApJ, 102, 168
Jordan C., 1988, in Viotti R., Vittone A., Friedjung M., eds, Proc. IAU Colloq. 94, Physics of formation of Fe II lines outside LTE. Reidel, Dordrecht, p. 223
Jordan C., 1991, in Ulmschneider P., Priest E. P., Rosner R., eds, Mechanisms of Chromospheric and Coronal Heating. Springer-Verlag, Berlin, p. 300
Kelemen J., 1985, Inf. Bull. Variable Stars, 2744, 1
Kholopov P. N., 1952, Perem. Zvezdy, 9, 157
Kholopov P. N., 1959, SvA, 3, 291
Königl A., 1991, ApJ, 370, L39
Lemmens A. F. P., Rutten R. G. M., Zwaan C., 1992, A&A, 257, 671
Linsky J. L., 1991, in Ulmschneider P., Priest E. P., Rosner R., eds, Mechanisms of Chromospheric and Coronal Heating. Springer-Verlag, Berlin, p. 166
Montmerle T., Feigelson E. D., Bouvier J., André P., 1993, in Levy E. H., Lunine J. I., eds, Protostars and Planets III. University of Arizona Press, Tucson, p. 689
Pearson K. J., King A. R., 1995, MNRAS, 276, 1303
Pérez M. R., 1991, ESA IUE Newsl., 38, 27
Phillips R. B., Lonsdale C. J., Feigelson E. D., ApJ, 1991, 382, 261
Rodonó M. et al., 1987, A&A, 176, 267
Rutten R. G. M., 1987, A&A, 177, 131
Rutten R. G. M., Schrijver C. J., Lemmens A. F. P., Zwaan C., 1991, A&A, 252, 203
Shu F., Najita J., Osriker E., Wilkin F., Ruden S., Lizano S., 1994, ApJ, 429, 781
Simon T., Vrba F. J., Herbst W., 1990, AJ, 100, 1957
Stickland D. J., 1980, ESA IUE Newsl., 5, 30
Tout C. A., Pringle J. E., 1992, MNRAS, 256, 269
Talavera A., Gómez de Castro A. I., 1987, A&A, 181, 300
Vrba F. J., Rydgren A. E., Chugainov P. F., Shakovskaya N. I., Zak D. S., 1986, ApJ, 306, 199
Yu K. et al., 1986, Astron. Tsirk., 1459, 5